Asociación Argentina
de Mecánica Computacional

Mecánica Computacional Vol XXVI, pp.2985-3004
Sergio A. Elaskar, Elvio A. Pilotta, Germán A. Torres (Eds.)
Córdoba, Argentina, Octubre 2007

COMPUTATION OF DYNAMIC LOADS OF WIND TURBINE POWER TRAINS

Andreas Heege, Jaume Betran, Loïc Bastard and Elisabet Lens

SAMTECH Ibérica, c/València 230, 08012 Barcelona, España, lisa.lens@samcef.com,
http://www.samcef.com

Keywords: wind turbines, aeroelasticity, fatigue computation, Nonlinear Finite Elements approach for flexible MultiBody Dynamics.

Abstract. The main concern of the present work is the computation of dynamic loads of wind turbine power trains, with particular emphasis on planetary gearbox loads. The applied mathematical approach relies on a nonlinear finite elements method, which is extended by multibody systems functionalities, and aerodynamics based on the Blade Element Momentum theory. The Finite Elements model used to simulate the behavior of wind turbines is introduced in detail. A comparison between numerical results and experimental data is shown. Fatigue diagrams by means of rainflow counting of load cycles and corresponding load duration distributions are also presented for some elements of the model.

1 INTRODUCTION

With a service life of about 20 years, wind turbine power trains are subjected to a very diverse spectrum of dynamic loads. Due to the high number of load cycles which occur during the life of a turbine, fatigue considerations are of particular importance in wind turbine design.

The respective load spectrum, in terms of load amplitudes and associated load cycles, depends on the dynamic properties of the complete mechatronical wind turbine system and cannot be calculated properly without detailed three-dimensional models. External excitations in terms of aerodynamic blade loads and electromagnetic generator torques, depend implicitly on control strategies for blade pitch and generator electronics, as well as on the general dynamic properties of the whole turbine. The purely dynamic character of certain gearbox loads, such as the axial loads on planet bearings, stresses the need for detailed dynamic power train models.

New standards for design and specification of gearboxes for wind turbines recommend to include all dynamic effects in the load computations (AGMA Foundation the American Gear Manufacturers Association, 2003; Germanischer Lloyd Windenergie GmbH, 2006; Cardona et al., 1991; Samtech SA, 2007). In order to cope with these requirements, the proposed fatigue procedure relies on a complete wind turbine model, which includes a detailed gearbox model. Accordingly, the load transients are extracted from the global model for each gearbox component and fatigue cycle counting is performed individually for each power train component. This procedure has the advantage that the frequency content and the associated amplitudes of the local transients take into account the nonlinear character of dynamic amplifications within the power train and respect the implicit dependence of the excitations on the dynamic properties of the entire mechatronical system. The fatigue load spectra, which are obtained from the global wind turbine model in terms of component wise load transients, take into account for local dynamic effects within the gearbox as well. Various topics will be dealt with as follows: First, a brief summary of the mathematical approach is presented. The methodology couples structures presented by the finite elements method (Géradin and Cardona, 2001; Bathe, 1982; Hughes, 1987; Géradin and Rixen, 1993), mechanisms and control loops using a multibody systems approach (Géradin and Cardona, 2001; Haug, 1989; Peeters, 2006) and aerodynamics in terms of Blade Element Momentum theory (Spera, 1994; Burton et al., 2001; Manwell et al., 2002). Some recommendations for the numerical analysis techniques involved in the computation of wind turbine power trains are given. Afterwards, a description of the aerodynamic-mechanical wind turbine model, including a detailed gearbox which is based on two planetary stages and one parallel helical stage is provided. Next, a grid loss event with subsequent emergency stop has been chosen as an example. Different aerodynamic results and detailed load transients for a gearbox with two planetary stages are presented. Then, the derivation of fatigue spectra of dynamic power train loads is given (Amzallag et al., 1994; Bishop and Sherratt, 1989b,a, 1990; Sutherland, 1994; Pitoiset, 2001). Fatigue diagrams of bearings are presented in terms of Rain Flow Counts (RFC) of bearing load cycles and corresponding Load Duration Distributions (LDD). Finally, the article ends with the study's conclusions.

2 COUPLING MECHANISM, STRUCTURAL ANALYSIS AND AERODYNAMICS

2.1 Prerequisites for numerical simulation of dynamic wind turbine power train loads

Wind turbine drive train loads are composed of loads which can be associated, on the one hand, with excitations induced by aerodynamic rotor blade loads and electro-magnetic generator torque and, on the other hand, with the proper dynamics of the entire dynamic system, including all control mechanisms. Decoupling of the dynamic wind turbine system into sub-systems

is difficult because dynamic coupling effects prevail during many operation modes. As a consequence, a coupled aerodynamic-mechanical approach is recommended for the evaluation of fatigue loads of highly dynamic events.

In order to cope with the above requirements, the following numerical modelling procedures might be particularly suitable:

- Nonlinear finite elements method (Géradin and Cardona, 2001; Bathe, 1982; Samtech SA, 2007) and super-element technique (Samtech SA, 2007; Craig and Bampton, 1968; Cardona and Géradin, 1991): blades, hub, rotor and gearbox shafts, further structural components like the bedplate, planet carriers, torque arms etc.

- Multibody systems approach (Haug, 1989; Peeters, 2006; Cardona et al., 1991): pitch and yaw drives, bearings of the entire power train including the generator, coupling elements for torque arms, high speed shaft coupling, clutches, the braking system, electromagnetic generator torque and finally controllers. Alternatively to the finite elements method, structural components restricted to small deformations can be represented by discrete assemblies of springs (generalized stiffness), masses and inertias.

- Aero-elastic computation procedures (Burton et al., 2001; Wilson and Lissaman, 1974; Anderson, 1984; Veers, 1988; Leishman and Beddoes, 1989; Øye, 1990; J. and A, 1991; Øye, 1996; Øye et al., 2003; Bossanyi, 2004): computation of consistent aerodynamic blade loads. The aero-elastic approach should be based on a strong coupling so that blade vibrations induced by aerodynamic forces implicitly affect the aerodynamics.

- Interface for external controller in terms of Dynamic Link Libraries (DLL) Bossanyi (2004) or suited user-programmable interface: blade pitch, generator torque, yaw regulation and further controller actions for reducing specific dynamic loads.

In some specific aero-elastic wind turbine programs (Øye, 1996; Bossanyi, 2004), a modal approach is used in order to present structural components like the blades, the tower and the rotor shaft. This approach is generally valid for small deformations, but less suited for the simulation of nonlinear phenomena like impacts in bearings and gears. In the case of blades which are subjected to large deformations, the modification of Eigen-frequencies, which can be either stress-induced, or related to large geometrical deformations, might be taken more naturally into account by a nonlinear Finite Element Method. However, both approaches have their inherent advantages.

In particular, in the presence of frictional contact problems like in the case of bearings and gears, the solver should be adapted to the solution of non-symmetric sets of equations (Samtech SA, 2007; Heege and Alart, 1996). Note that anisotropic blade properties, gyroscopic effects and finally radial-axial-bending coupled bearing stiffness functions also produce a non-symmetric coupling of global equilibrium equations.

By knowing that wind turbine fatigue load analysis requires the simulation of time intervals, which are frequently longer than $5000\ \mathrm{s}$, an implicit, unconditionally stable, time integration scheme is indicated (Goudreau and Taylor, 1973; Belytschko, 1983; Cardona and Géradin, 1989; Cassano and Cardona, 1991; Thomas and Gladwell, 1988; Gladwell and Thomas, 1988). In order to preserve numerical stability of an explicit, conditionally stable, time integration procedure, the maximum time step is limited by a fraction of the time period, which is associated to the highest frequency of any component of the wind turbine. This limitation on the time step

size of explicit integration schemes is also valid if higher frequencies are not excited. As a consequence, in comparison to implicit integrators, this limitation on the time step size of explicit integration procedures results in excessive computation times.

2.2 Nonlinear Finite Elements approach for flexible MultiBody Dynamics

The applied mathematical approach (Géradin and Cardona, 2001; Samtech SA, 2007) is based on a nonlinear Finite Element formalism, which accounts for flexible multibody systems functionalities, control devices and aerodynamics in terms of the Blade Element Momentum Theory simultaneously.

The linearized form of the time equations of motion to solve are:

$$\begin{bmatrix} \boldsymbol{M} & \boldsymbol{0} \\ \boldsymbol{0} & \boldsymbol{0} \end{bmatrix} \begin{bmatrix} \Delta\ddot{\boldsymbol{q}} \\ \Delta\ddot{\boldsymbol{\lambda}} \end{bmatrix} + \begin{bmatrix} \boldsymbol{C} & \boldsymbol{0} \\ \boldsymbol{0} & \boldsymbol{0} \end{bmatrix} \begin{bmatrix} \Delta\dot{\boldsymbol{q}} \\ \Delta\dot{\boldsymbol{\lambda}} \end{bmatrix} + \begin{bmatrix} \boldsymbol{K} & \boldsymbol{B}^T \\ \boldsymbol{B} & \boldsymbol{0} \end{bmatrix} \begin{bmatrix} \Delta\boldsymbol{q} \\ \Delta\boldsymbol{\lambda} \end{bmatrix} = \begin{bmatrix} \boldsymbol{r}(\boldsymbol{q},\dot{\boldsymbol{q}},t) \\ -\boldsymbol{\Phi}(\boldsymbol{q},t) \end{bmatrix} + O(\Delta^2) \qquad (1)$$

Note that the stiffness matrix $\boldsymbol{K}$, the damping matrix $\boldsymbol{C}$, the mass-inertia matrix $\boldsymbol{M}$, the residual vector $\boldsymbol{r}(\boldsymbol{q},\dot{\boldsymbol{q}},t) = -\boldsymbol{g}(\boldsymbol{q},\dot{\boldsymbol{q}},t) - \boldsymbol{M}\ddot{\boldsymbol{q}} - \boldsymbol{B}^T\boldsymbol{\lambda}$ and constraint Jacobian matrix $\boldsymbol{B} = \partial\boldsymbol{\Phi}/\partial\boldsymbol{q}$ show nonlinear dependency on the generalized solution vector:

$$\begin{Bmatrix} \boldsymbol{q} \\ \boldsymbol{\lambda} \end{Bmatrix}_{t_{n+1}}^{i+1} = \begin{Bmatrix} \boldsymbol{q} \\ \boldsymbol{\lambda} \end{Bmatrix}_{t_n} + \begin{Bmatrix} \Delta\boldsymbol{q} \\ \Delta\boldsymbol{\lambda} \end{Bmatrix}_{t_{n+1}}^{i+1}$$

Vector $\boldsymbol{g}(\boldsymbol{q},\dot{\boldsymbol{q}},t)$ presents the sum of internal, external and complementary inertia forces where centrifugal and gyroscopic effects are included. Vector $\boldsymbol{\Phi}$ introduces additional equations of solution $\boldsymbol{\lambda}$, which is used to include general multibody systems functionalities, aerodynamics and controller constraints. Note that the applied solver SAMCEF-Mecano solves the equations (1) by means of the Hilber-Hughes and Taylor scheme (Hilber et al., 1977; Cardona and Géradin, 1989).

Concerning the computational implementation, the main numerical difficulties are the iterative solution of the nonlinear equations (1) and the time integration procedure Cardona and Géradin (1989, 1994); Lens (2006); Lens and Cardona (2007). Further details on time integration procedure, error estimators and solution strategies for equation solvers, can be found in the SAMCEF-Mecano user manual (Samtech SA, 2007).

2.3 Aerodynamic Blade Section Elements for wind loads

Bearing in mind that blades are represented by super-elements or nonlinear beam elements respectively, the Blade Element Momentum theory can be applied very efficiently in order to introduce the wind loads by Aerodynamic Blade Section Elements.

The Blade Element Momentum theory can be considered as a two-dimensional approach, which models the interaction of the incoming wind with an annular segment covered by the rotating blades. The model is based on the inviscid momentum theory of fluid dynamics and hence Blade Element Momentum can be looked upon as a simple potential flow model. The momentum theory refers to the conservation of linear and angular momentum, which directly follows from Newton's second law of motion (Burton et al., 2001; Spera, 1994; Heege et al., 2006a; Wilson and Lissaman, 1974).

As depicted in Figure 1, the discretisation of aerodynamic loads corresponds to the structural discretisation in terms of retained super-element nodes or, respectively, beam nodes.

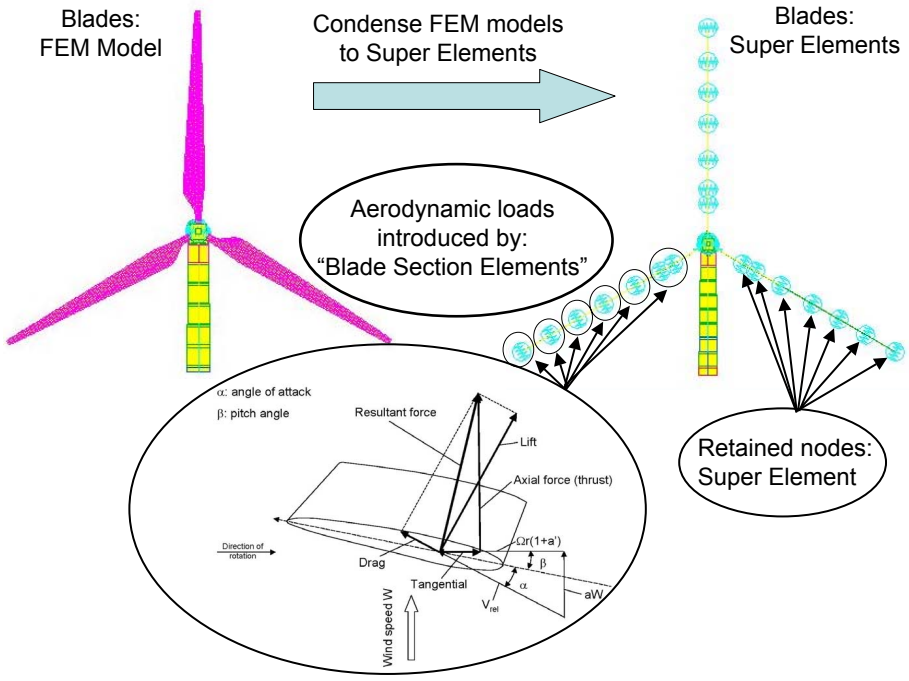

Figure 1: Modelling of blades by super-elements and aerodynamic blade section elements.

Aerodynamic loads are introduced by *Finite Blade Section Elements* which contribute in terms of elemental aerodynamic forces to the global equilibrium equation (1). The actual blade geometry is discretized by surface contributions A_I, which correspond to the airfoil span times the chord length of section I. The three-dimensional shape of wind turbine blades is accounted for by local blade section twist Ψ^I and coning angles θ^I. Twist and coning angles are introduced in terms of local blade section coordinate systems which are attached to each blade node. According to twist and coning angles, blade section coordinate axes are aligned with the tangential and normal directions of the respective blade section and follow any deformation or rotation of the blades naturally.

Actual wind loads are computed with respect to a wind coordinate system the orientation of which is a priori an unknown, because it is rotated with respect to the associated local blade section coordinate systems by the unknown angles of attack α^I. The angles of attack α^I depend implicitly on the unknown induced velocities at each blade section, and thus on the solution of the global constraint field problem (1).

Aerodynamic force components can be stated in the a-priori unknown wind coordinate system by the classical expression:

$$\boldsymbol{F}^I_{lift} = \frac{1}{2} C^I_{lift}(\alpha^I) \rho \boldsymbol{V}^2_{rel_I} A_I \quad \boldsymbol{F}^I_{drag} = \frac{1}{2} C^I_{drag}(\alpha^I) \rho \boldsymbol{V}^2_{rel_I} A_I \quad \boldsymbol{M}^I_{pitch} = \frac{1}{2} C^I_{M}(\alpha^I) \rho \boldsymbol{V}^2_{rel_I} A_I \tag{2}$$

Whereas the lift force $\boldsymbol{F}^I_{lift}$ acts normally to the relative wind velocity vector, $\boldsymbol{F}^I_{drag}$ the drag force, acts perpendicularly in the direction of the relative wind velocity. The torque generated with respect to the blade pitch axis is denoted $\boldsymbol{M}^I_{pitch}$. Lift, drag and moment coefficients, denoted $C^I_{lift}(\alpha^I)$, $C^I_{drag}(\alpha^I)$ and $C^I_M(\alpha^I)$ are functions of the angle of attack. Note that the relative velocities $\boldsymbol{V}_{rel}$ account for the induction corrections due to the global flow interaction with the blades and have to satisfy the constraints which are stated in Equations (3).

In order to couple equations (2) and (3) to the global field problem of equation(1), the induction factor for speed normal to the rotor plane (denoted: a), and the induction factor for speed

tangent to the rotor plane (denoted a') , can be obtained from equations (3). In that context, Ω_r represents the unperturbed tangential rotor plane speed at blade section I of radius r, Φ presents the angle between relative wind vector and plane of rotation and W represents the unperturbed wind speed normal to the rotor plane:

$$\begin{aligned}
a'(1+a')x^2 &= a(1-a)\cos^2\theta && \text{tip speed ratio, with } x = \Omega r/W \\
C_t &= 4aF(1-a) && \text{thrust coefficient for } a \leq a_c \\
C_t &= 4F[a_c^2 + (1-2a)a] && \text{thrust coefficient for } a > a_c \\
a_c &= 0.2 && \text{empirical constant} \\
F &= \frac{2}{\pi} ar\cos\left(\exp\left(-\frac{B(R-r)}{2r\sin\Phi}\right)\right) && \text{Prandtl tip loss factor}
\end{aligned} \tag{3}$$

According to the Wilson and Walker approximation (Spera, 1994; Burton et al., 2001; Manwell et al., 2002; Wilson and Lissaman, 1974; Anderson, 1984; Veers, 1988) for the thrust of an annular rotor segment, one can write the equality of the thrust coefficient C_t^I and the projection of the aerodynamic lift and drag loads on the rotor plane: $C_t^I = Proj|_{rotorplane}[\boldsymbol{F}_{lift}^I, \boldsymbol{F}_{drag}^I]$ thus coupling equations (1), (2) and (3). Taking into account that the aerodynamic loads $[\boldsymbol{F}_{lift}^I, \boldsymbol{F}_{drag}^I, \boldsymbol{M}_{pitch}^I]$ presented in equation (2) are included in the internal forces of vector $\boldsymbol{g}(\boldsymbol{q}, \dot{\boldsymbol{q}}, t)$ of equation (1), once the iterative solution of coupled equations (1), (2) and (3) is found, the induced velocities, angles of attack, Prandtl's tip loss coefficients and local aerodynamic forces are consistent.

It is emphasized that the methodology applied permits a strong coupling, i.e. all equations associated either with aerodynamics, structures, mechanisms, or control loops are solved simultaneously. A major advantage of a strong coupling is that blade vibrations induced by aerodynamic forces implicitly affect the latter.

2.4 Tower shadow and wind shear

Before computing the proper induced velocities at the different blade sections, some adjustments are performed beforehand on the unperturbed wind field. First, the unperturbed speeds of the three-dimensional turbulent wind field are adjusted in order to take into account the velocity gradient induced by ground effects and then, secondly, to account for the impact of the tower shadow.

In order to account for the wind shear close to the ground, the wind speed is written as an exponential function of the relative height h of a blade section node with respect to the rotor hub height h_{hub}. The incoming, unperturbed wind speed $\boldsymbol{V}_\infty$ is taken as reference at the rotor hub and is corrected by an exponential law yielding the wind speed without induction, $\boldsymbol{V}(h)$ as a function of ground distance $\boldsymbol{V}(h) = \boldsymbol{V}_\infty(h : h_{hub})^{Shearcoeff}$. The impact of the tower on the unperturbed wind field is modelled by classical non-lifting flow theory over a circular cylinder (Anderson, 1984). An analytical solution for the radial flow V_r and tangential flow V_Θ is obtained from the stream function Ψ as function of azimuth angle Θ and tower distance $\boldsymbol{r}$

$$V_r = \frac{1}{r}\frac{\partial \Psi}{\partial \Theta} \quad V_\Theta = -\frac{\partial \Psi}{\partial r} \quad \text{with} \quad \Psi = \boldsymbol{V}_\infty \boldsymbol{r}\sin\Theta(1 - R_{tower}^2/r^2)$$

The proper computation of the induced velocities at the blade sections is performed after the cited corrections on the unperturbed wind field.

It is anticipated that the presented aerodynamic model is a basic implementation of Blade Element Momentum theory, which was initially developed for steady state applications. Future enhancements might concern the implementation of dynamic stall models such as the Leishman-Beddoes model (Leishman and Beddoes, 1989), more advanced models for the computation of aerodynamic induction and more realistic wake models (Øye, 1990; Øye et al., 2003).

3 STRUCTURAL AND MULTIBODY SYSTEMS MODELLING OF A WIND TURBINE

Structural components, which are subject to elastic deformations and which have impact on the dynamic properties, are included in the complete wind turbine model in terms of finite elements models. Taking into account that long time intervals (longer than $1000\ \mathrm{s}$) have to be analyzed, the total number of degrees of freedom of the complete analysis model should stay below 10000 degrees of freedom. As a consequence, the *finite elements structures*, which are subject only to small deformations, are condensed by the super-element technique. The rotor shaft, all gearbox shafts, the generator rotor and the tower are modelled by nonlinear beam elements.

Further flexible *mechanism type components* like gears, bearings, drive train couplings and generator mechatronics are introduced through a multibody systems approach in terms of additional degrees of freedom of the global equilibrium equation (1).

3.1 Damping modelling

Stiffness proportional damping (Géradin and Cardona, 2001; Géradin and Rixen, 1993; Samtech SA, 2007) is applied to all structural components, which are presented either by beam elements or by super-elements. The amount of damping is set for all components to 2% critical damping, except for the composite material blades where 4% of critical damping is applied. Viscous damping, or respectively Coulomb friction, is applied to every bearing and gear contact (Samtech SA, 2007). In the case of torque arm coupling elements, a nonlinear deformation speed dependant viscous law is applied.

Note that the aerodynamic loads can also be considered as damping forces, because aerodynamic laws of type of equation (2) are essentially related to speeds.

3.2 Gearbox modelling: coupled multibody systems and finite elements approach

The gearbox is included in the global analysis model combining finite elements and multibody systems approaches. All gearbox shafts, including the rotor shaft, are represented by nonlinear beam elements. The gearbox housing and the planet carriers are modelled by solid finite elements models, which are condensed to super-elements in order to reduce the number of degrees of freedom.

Frictional contact problems between flexible gears are reduced to geometrically variable and point wise flexible contacts. Gear geometry is defined by helix, cone and pressure angles, normal modulus, respective teeth number and, if needed, further correction factors for the gear teeth. In context of noise prediction, geometric imperfections (typically due to manufacturing tolerances) can be included in the analysis model in terms of geometrical transmission error. Gear teeth flexibility is defined by nonlinear gap-functions, which account for stiffness variation, when passing along one tooth engagement. It is emphasized that the proper modelling of gear and bearing clearances is of crucial importance when evaluating gearbox loads during

backlashes. The so-called parameter-excitation (nonlinear gear teeth contact stiffness functions) can be defined in terms of Fourier series containing as many harmonics as necessary to describe the stiffness variation when passing along one tooth engagement (Samtech SA, 2007; Cardona, 1997; Cardona and Granville, 1999). That extension of the gear tooth flexibility is necessary in order to reproduce the higher frequency content generated by the teeth engaging properly.

Every bearing of the wind turbine, including those of the rotor main shaft, the entire gearbox and the generator, is modelled by nonlinear stiffness functions, which account for the coupling of radial and axial bearing properties. All bearing clearances in radial and axial directions are taken into account.

3.3 Some remarks about the use of super-element techniques

Most commercial multibody systems or finite elements programs support the use of super-elements. Some super-element formulations are based on the Guyan condensation, whereas more advanced super-element formulations rely on the Component synthesis Method (CSM) and take into account nonlinearities of large rotations, centrifugal and gyroscopic forces.

Generally speaking, the use of super-element should be limited to structural components which are being subjected to only small deformations. The structural behaviour of super-elements is linear within a rotating reference frame, i.e. super-elements do not take into account material nonlinearity, nor nonlinearity related to large deformations. As a consequence, super-elements do not take into consideration stress-induced nonlinearity, such as blade stiffening under loading.

If the modification of blade eigenfrequencies as a function of loading has to be considered, a nonlinear finite element approach seems to be the most natural choice.

If structural components are modelled by super-elements, compared to discrete assemblies of springs, masses and inertias, less discretization in terms of retained nodes is required. In comparison to sparse stiffness, damping and mass matrices of discrete spring-mass assemblies, the fully occupied matrices of super-elements contain more information on eigenmodes and on structural coupling effects. If the super-elements are based on a CSM formulation, the frequency content can be easily further enhanced by additional internal modes (Samtech SA, 2007; Craig and Bampton, 1968; Cardona and Géradin, 1991).

3.4 Controllers for blade pitch, generator torque and yaw angle

Generally, an external Dynamic Link Library/DLL is coupled to SAMCEF in order to define the electro-mechanical generator torque, the demanded yaw angle and the demanded blade pitch angle as a function of control variables like the rotor speed and torque. Alternatively, a standard PID controller of SAMCEF is applied, as in the present example. Note that the controller demand of a given pitch angle is further processed in order to include the mechanical response of the proper pitch drive and controller. Accordingly, the mechanical pitch drive is limited by maximum pitch speed and acceleration.

4 APPLICATION EXAMPLE: EMERGENCY STOP

Figures 1, 2 and 3 show schematically the applied wind turbine model including, on the one hand, *structural finite elements components* like blades, rotor and gearbox shafts, the tower structure, gearbox housing, planet-carriers, bedplate etc. and, on the other hand, *multibody systems type components* like gears, bearings, elastic couplings or bushings, the overload clutch, and finally the generator model and control loops. The model presents a configuration for

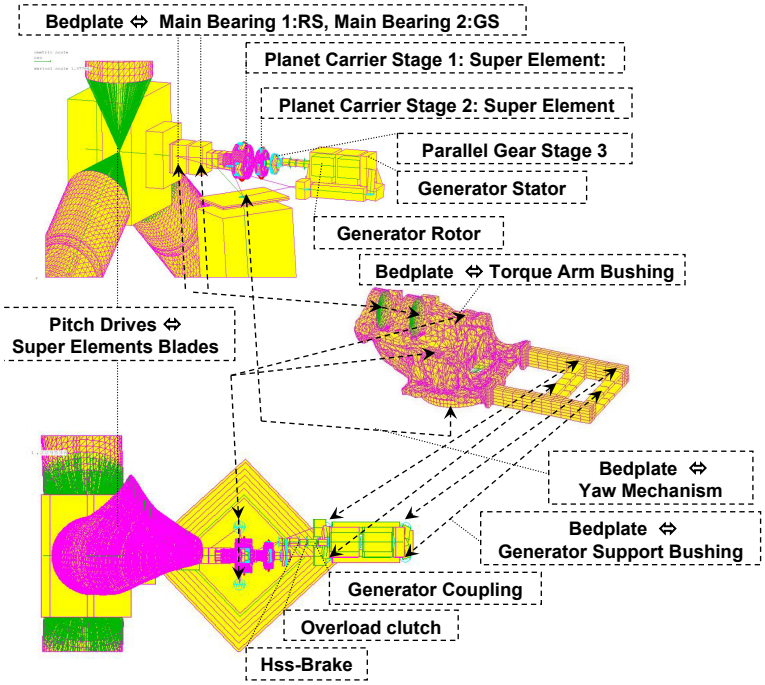

Figure 2: Modelling of blades by super-elements and aerodynamic blade section elements.

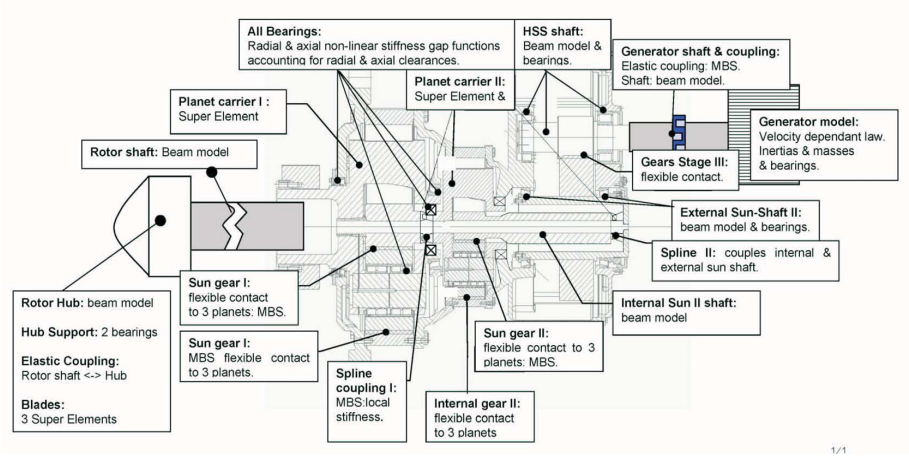

Figure 3: Modelling of blades by super-elements and aerodynamic blade section elements.

approximately $4.5\ \mathrm{MW}$ nominal power output at rotor speed of $13.5\ \mathrm{rpm}$. Rotor diameter is $118\ \mathrm{m}$ and the tower height is $112\ \mathrm{m}$. As depicted schematically in Figure 3, the gearbox model is based on two planetary stages and one parallel helical stage, where the numerical model accounts for every relevant gearbox component. Gear geometries, clearances and mechanical properties are adapted according to a commonly applied wind turbine gearbox configuration of a total transmission ratio of ninety-five.

4.1 Emergency stop: aerodynamic results

Our first numerical example is an emergency stop simulation. Emergency stop, or E-stop, is the process that brings the wind turbine to rest as fast as possible. The control system orders an E-stop in the case of grid loss, excessive vibrations etc. In the presented example, the E-stop is triggered by a grid loss event which is characterized by a sudden drop in generator torque due

to an electrical failure. As a consequence, the pretension of the power train is lost and large dynamic oscillations occur. These oscillations frequently produce backlashes.

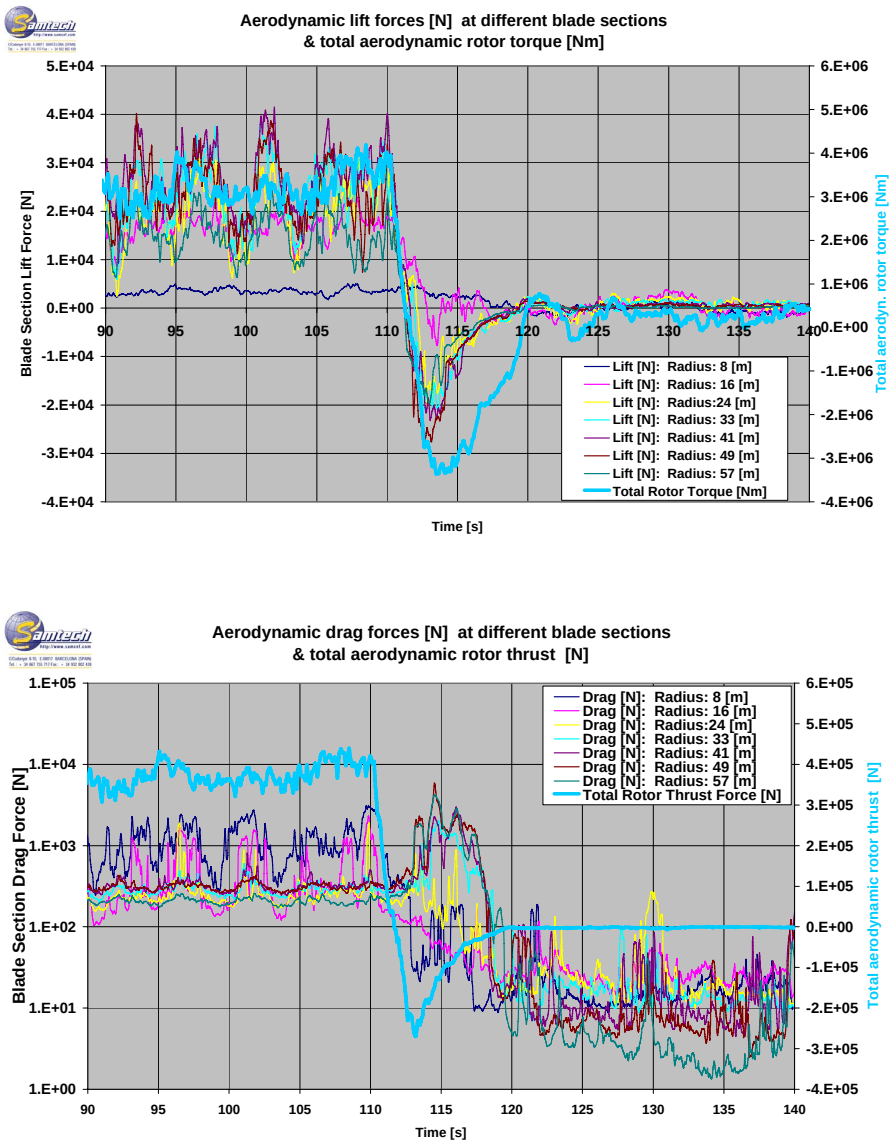

Figure 4: (a) Lift forces [N] for different blade sections and total aerodynamic rotor torque [Nm]. (b) Drag force [N] for different blade sections and total aerodynamic rotor thrust [N]

Preventive measures, such as immediate pitching and activation of the disc brake, must be taken in order to ensure the wind turbine does not run into excessive over speed.

The aerodynamic results of the emergency stop depicted in Figure 4 correspond to a mean wind speed of $14\ \mathrm{m/s}$ with turbulence intensities according to $IEC\ 61400-1$ standard (International Electrotechnical Commission, 1997), i.e. a turbulence intensity of 18% in incoming wind direction. Turbulence intensities in lateral and vertical directions are 15% and 10% respectively.

Figure 5 presents the rotor shaft torque, the torque in the high speed shaft coupling (located at the gearbox exit), the disc brake and finally the electro-magnetic generator torque. Note that

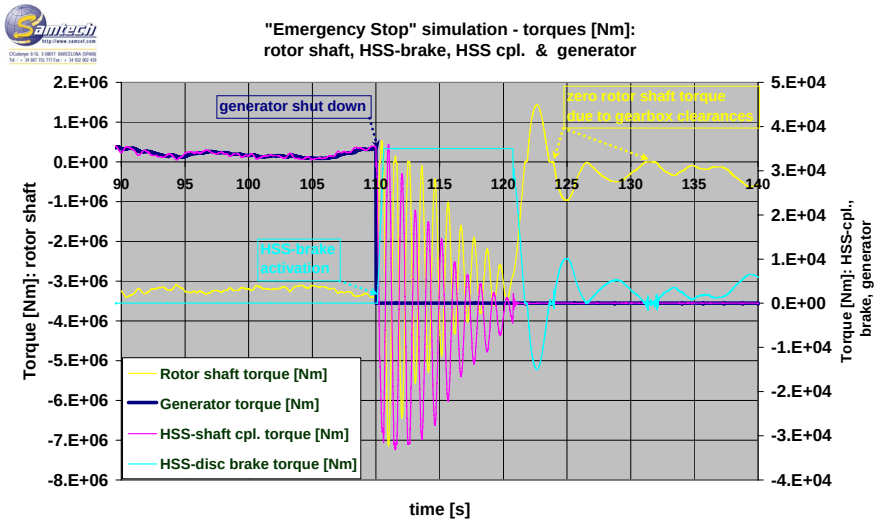

Figure 5: Torques [Nm] of rotor main shaft (left ordinate), brake at gearbox exit, high speed shaft coupling and generator

rotor shaft torque refers to the left ordinate and that remaining torque plots refer to the right ordinate of Figure 5.

As shown in the pink plot of Figure 6, blade pitch is nearly constant up to time $t = 110\,\mathrm{s}$. In the following $10\,\mathrm{s}$, in order to reverse the rotor torque, the blade is pitched about 1.5 [rad] away from the rotor plane in the wind. Figure 6 shows the pitch angle (left ordinate), the rotor shaft speed (left ordinate) and finally the high speed shaft speed (right ordinate).

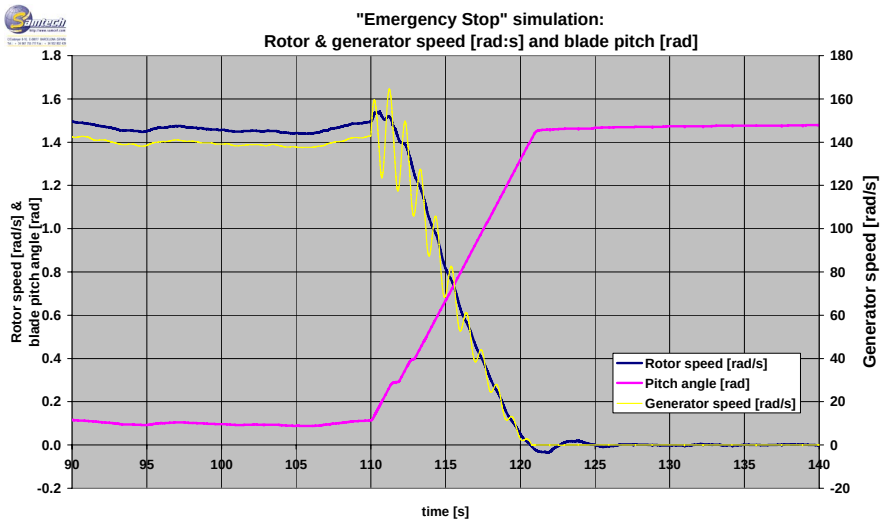

Figure 6: Rotor speed [rad/s], blade pitch angle [rad] and generator speed [rad/s] (right ordinate)

It is assumed that generator disconnection takes place at the time instance $t = 110\,\mathrm{s}$ and activation of the disc brake is delayed by $0.01\,\mathrm{s}$. After activation of the disc brake, braking torque is augmented in $0.5\,\mathrm{s}$ from zero to full torque of $35000\,\mathrm{Nm}$.

Lift and drag forces are depicted for different blade sections in Figures 4 with respect to each individual local, a priori unknown, blade section co-ordinate system. These local co-ordinate systems are rotated individually as function of the, a priori unknown, angles of attack where proper blade vibrations are taken into account when computing induced velocities.

In Figures 4, there is also shown the resulting total aerodynamic torque and thrust, presented by the light blue plots which refer to the right ordinates of respective figures. Plots of total aerodynamic torque and total aerodynamic thrust are derived a-posterior to the computation by means of transformations of local lift and drag forces to the rotor plane co-ordinate system.

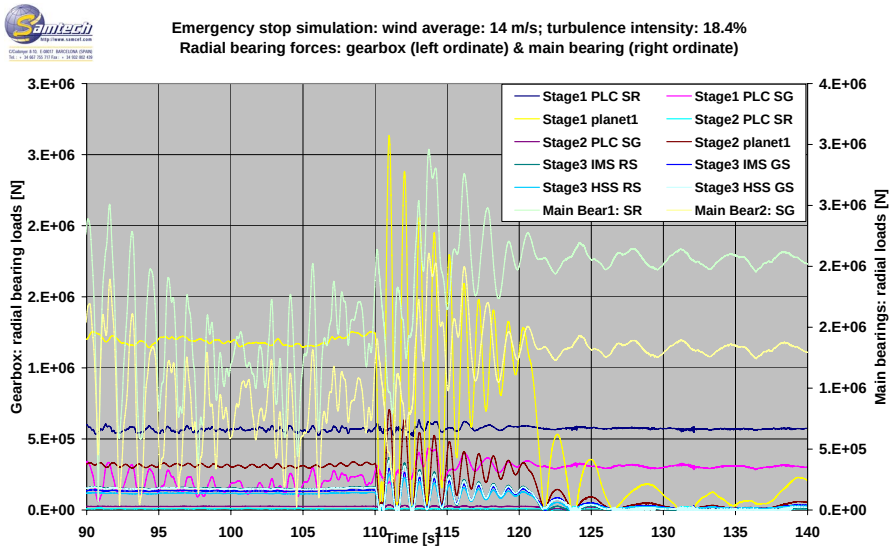

Figure 7: Radial bearing forces [N]

4.2 Dynamic load transients in rotor main bearings and in gearbox during emergency stop

Figures 7 and 8 present the radial and axial bearing forces of each rotor main bearing and of each planetary gearbox bearing. Figure 9 depicts the gear forces.

It is emphasized that the dynamic radial and axial bearing load oscillations of the individual power train bearings are not necessarily proportional to the power train torque. Note that the amplitudes of transient loads during the grid loss depend highly on control actions and details of the power train design, such as bearing clearances.

4.3 Comparison of numerical results to experiments and other aero-elastic programs

Previously, numerical results of several wind turbine models of the mega-watt class, all based on identical modelling procedures and solver technology (Heege et al., 2006a; Heege, 2005; Heege et al., 2006b), were compared to experimental measurements. In particular, measurements were compared to numerical results for specific manoeuvres like grid loss events, emergency stops and operation under turbulent wind conditions. The type of transients that were compared were rotor and high speed shaft torques, deformations in the gearbox torque arm bushings, global accelerations at specific locations like the tower top and finally blade root bending moments. For the investigated cases, wind turbine models could be tuned so that

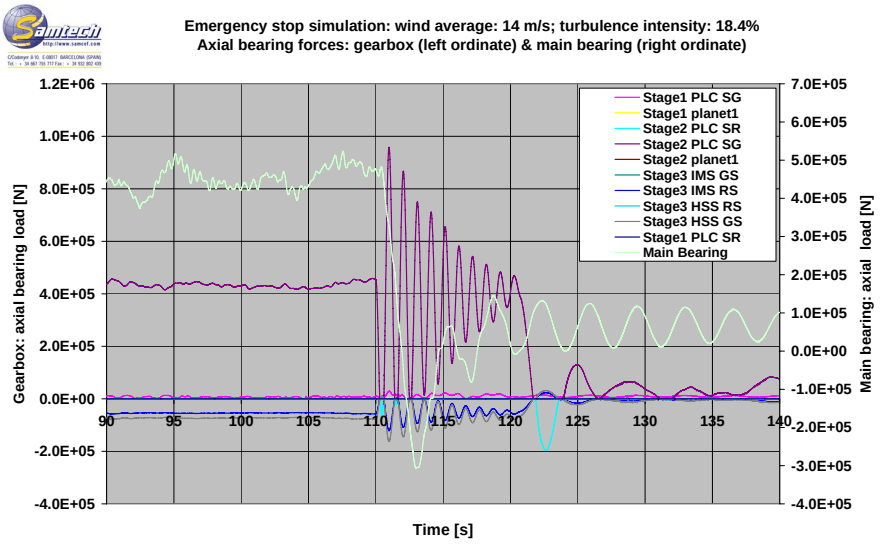

Figure 8: Axial bearing forces [N]

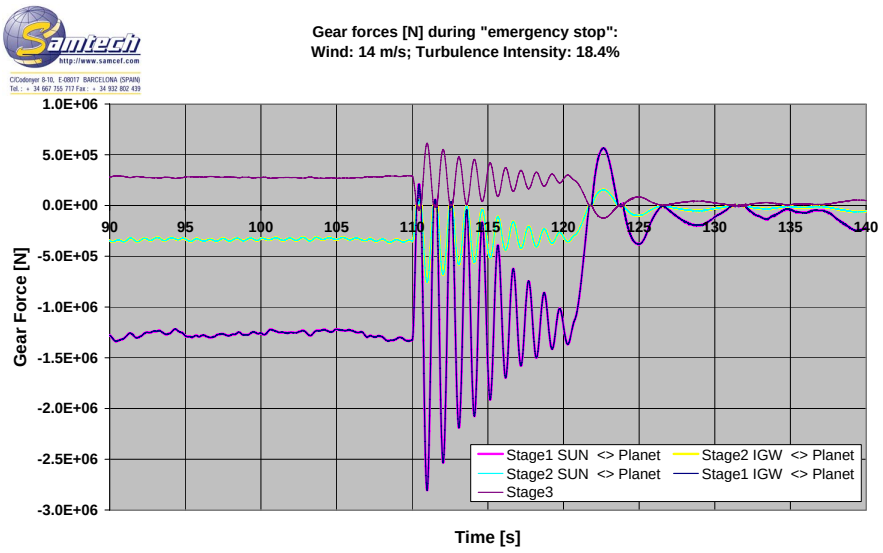

Figure 9: Gear forces [N]

numerical results and available experimental data showed generally less than 30% deviation. Within the gearbox, axial dynamics of several shafts were recorded experimentally and some of the results are shown as follows in Figure 11. This figure presents the comparison of numerical and experimental data for the axial vibrations of the parallel helical shaft of the second gear stage during different emergency stops where different brake torques at the gearbox brake exit are applied. Note that these measurements are obtained from a three-stage parallel gearbox of a 750kW class wind turbine.

Figure 10 compares the numerical rotor shaft torque results with corresponding experimental data during an emergency stop at low wind conditions. The experimental and numerical data refer to a simulation model of a 1.5 MW class wind turbine. The sudden augmentation of rotor

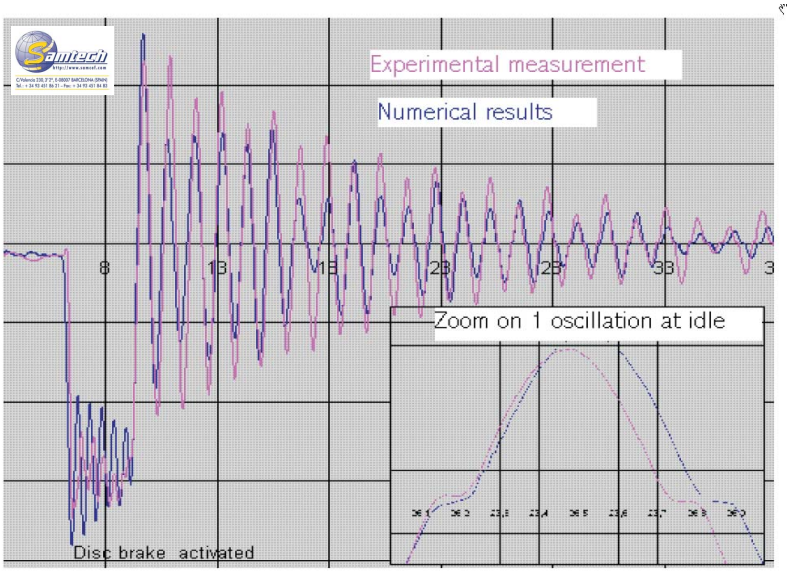

Figure 10: Comparison to experiment, Main shaft torque [Nm].

shaft torque at about time 6 s is due to the activation of the disc brake at the gearbox exit. It can be seen that the numerical model reproduces with very satisfactory precision the system change which occurs at the transition from *brake disc slipping* to *brake disc arrested* state. During the time interval from $t = 6$ s to $t = 10$ s, the first drive train mode is visible at about 1.7 Hz. These oscillations of 1.7 Hz correspond to the pre-tensioned power train with all gears and bearings in contact. After $t = 10$ s, the turbine is nearly at rest, only the rotor keeps oscillating slightly, but the disc brake is still closed. Now the dominating frequency drops to about 0.8 Hz, because the pre-tension of the power train is substantially reduced or completely lost. Figure 10 also includes a zoom on one single rotor shaft torque oscillation with the disc brake arrested. The comparison to experimental data shows that the numerical model reproduces the zero torque instances which are produced by radial, axial and gear clearances during load inversion.

Concerning the validation of the proposed numerical procedures, results of global aerodynamic rotor torques and thrust forces were compared, for different wind turbines, with further aero-elastic computer programs (Øye, 1996; Bossanyi, 2004). Generally, deviations in total aerodynamic rotor thrust and torque were less than 15% for investigated aerodynamic load cases including turbulent three-dimensional wind fields.

5 FATIGUE EVALUATIONS

Power train bearing failures occur more frequently than damage to the other components (Johnsen, 2004). Taking into account that these failures occur to a certain degree after a couple years of successful operation, the importance of proper fatigue considerations becomes obvious (Amzallag et al., 1994; Bishop and Sherratt, 1989b,a, 1990).

In widely used design practices of gearboxes, fatigue evaluations are based essentially on the time history of the rotor shaft torque. Looking at the transient curves depicted in Figures 4-9, it can be seen that this design practice is only of very limited precision, because of the nonlinear dynamic load amplification within the gearbox, which cannot be simulated with traditional aero elastic computer programs. More precise load spectra for the different gearbox components are

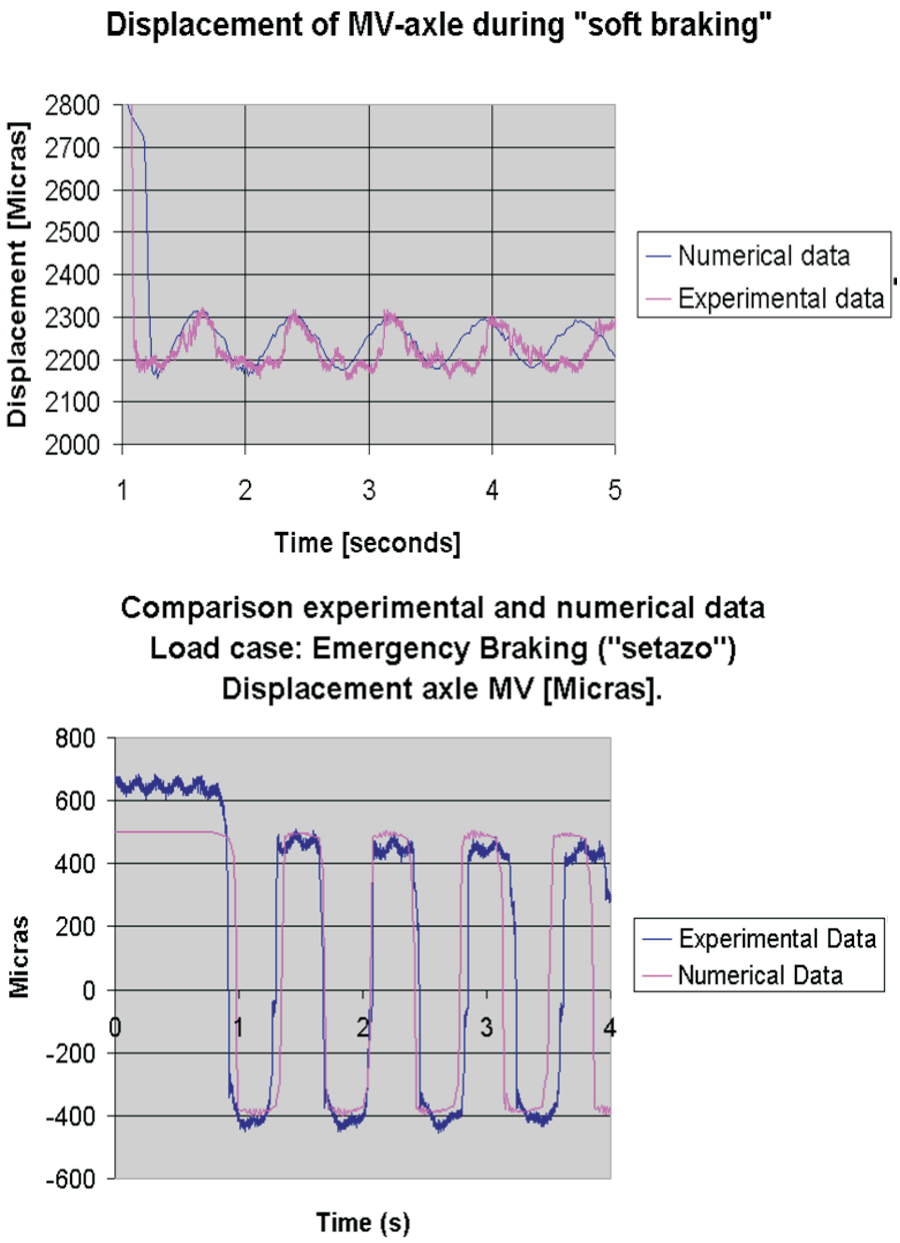

Figure 11: Comparison to experiment: axial shaft displacement [μ m] versus time s (a) at low brake torque and (b) at full brake torque.

obtained if the nonlinear dynamic load amplifications are introduced component wise in order to correct the input quantities in terms of rotor shaft time histories. However, this approach only corrects the loads amplitudes seen by each power train component, but no correction for the associated load frequencies is considered.

In order to further improve the fatigue load spectra of power train components, Rain Flow Counting (RFC) and Load Duration Distributions (LDD) are extracted separately for each gearbox component. This approach implies that transient loads are extracted for each power train component from the global mechatronical wind turbine model and that RFC and/or LDD evaluations are performed separately for each bearing and gear of the power train. This procedure has the advantage that the frequency content and the associated amplitudes of the local transients take into consideration the nonlinear character of dynamic amplifications within the power train

and respect the implicit dependence of the excitations on the dynamic properties of the entire mechatronical system. Accordingly, the fatigue load spectra also consider local dynamic effects within the gearbox, in particular those occurring during gearbox resonance.

In the case of structural components, finite elements models might be used in order to compute the stress state associated with each load cycle and corresponding load case. Let us point out that structural components like blades or bedplate are included in the global mechatronical wind turbine model, but condensed by the super-element technique in order to reduce CPU time. Accordingly, the stresses within the structural components can be recovered at any instance of the transient analysis, by a back-transformation from the condensed super-element to the original complete finite elements model (Samtech SA, 2007). In that case, the boundary conditions for the finite elements components are obtained automatically from the global wind turbine model. If Wöhler fatigue curves are available, the damage of the respective structural component can be computed using Miner's rule. Bearings and gears are modelled by a multibody systems approach, thus reducing the analysis results to three-dimensional load transients at the respective contact points. These load transients might be used as input data for specific programs for fatigue computations of gears or bearings.

As an example, figure 12-a presents the radial bearing load cycles in terms of RFC's individually for each bearing. The RFC's are obtained by gathering some relevant load cases and multiplying the obtained cycle numbers so that RFC fatigue results are extrapolated to 20 years of operation. Analogously, figure 12-b presents the cumulated radial bearing load duration distribution so that evaluated LDD fatigue results are extrapolated to 20 years of operation. It is emphasized that the selected load cases include exclusively non-stationary operation under turbulent wind conditions for a sub-set of wind speeds according to $IEC\ 61400-1$ specifications (International Electrotechnical Commission, 1997). The selected wind speeds are from $6\ \mathrm{m/s}$ to $22\ \mathrm{m/s}$ with turbulence intensities in wind, lateral and horizontal directions according to $IEC\ 61400-1$ specifications. Accordingly, the load spectra presented in Figure 12 do not include any extreme events, neither any non-operational load cases, neither any machine fault state (AGMA Foundation the American Gear Manufacturers Association, 2003; Germanischer Lloyd Windenergie GmbH, 2006).

It is important to realize that all presented results might differ slightly from loads in practice for diverse reasons. Damping mechanisms of composite blades or of elastic torque arms couplings are complex and experimental data for model characterization is not always available. Suitable data for mechanical characterization of coupling and damping effects in bearings are difficult to obtain. Aerodynamic models might to be further improved for strongly turbulent wind conditions. A further source for deviations in between presented numerical and real field load spectra might result from eventual defects which are not accounted in the numerical model. These defects might be power train misalignments, loss of pre-tensions in coupling elements, augmentation of bearing clearances during operation, or vibrations induced by small individual blade pitch errors. In the presented fatigue results, possible machine faults, or special events like grid loss, emergency stops, etc. are not taken into account. As a consequence, loads in practice might be potentially higher than presented in Figures 12.

6 CONCLUSIONS

The implicit dependence of power train loads on the dynamic characteristics of the assembled wind turbine turns out difficult a decoupling of analysis techniques, in order to reduce the complexity of the numerical models. If a gearbox is analysed without accounting for the other properties of the wind turbine, there is some risk that cycle count, as well as load amplitudes

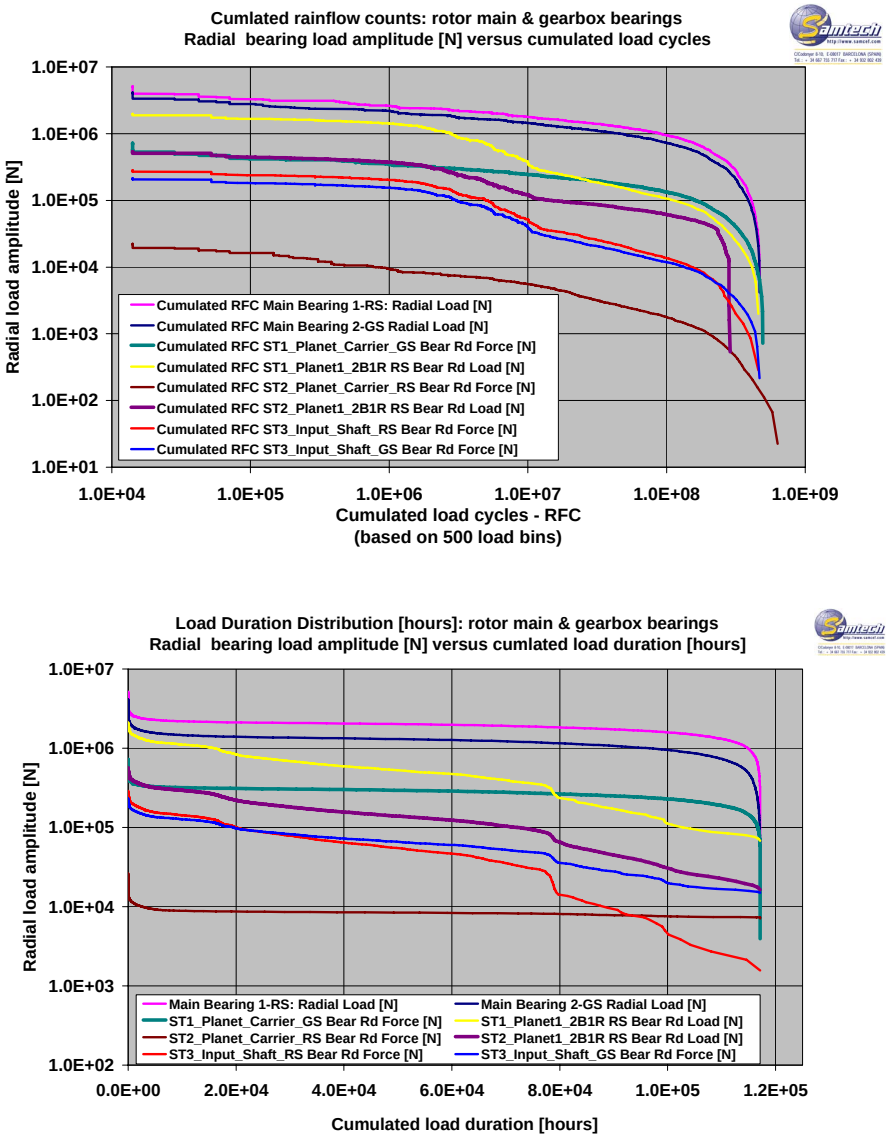

Figure 12: Radial bearing load [N] versus (a) cumulated RFC-load cycles and (b) cumulated LDD's (hours).

are underestimated. For highly dynamic operation modes, possible operation deflection modes might affect the alignment of the power train and should be taken into account in fatigue evaluations. In particular if backlashes occur, the load amplifications within the gearbox are generally much larger than the amplifications which would be detected by experimental measurement or numerical simulation at the rotor shaft and the high speed shaft.

The need for complete, fully coupled, three-dimensional models is further emphasized by the purely dynamic character of certain gearbox load components, such as the axial loads of planet bearings, or the axial and radial bearing loads of the first planet carrier. Dynamic operation modes, which result in important vibrations of the entire power train are frequently producing combined radial, bending and axial loads in the first planetary stage bearings. These kind of dynamic loads are difficult to capture by too simplified computational methods.

In the case of fatigue considerations being based only on rotor shaft time history, the introduction of dynamic load amplitude and load cycle correction factors for different gearbox

components and for different load directions might allow for improved fatigue calculations. However, due to the nonlinear and three-dimensional character of wind turbine dynamics, it is recommended that the respective Load Duration Distribution and/or Rain Flow Counts be extracted from a global dynamic model individually for each power train component. This requirement leads to the use of implicitly coupled analysis techniques like the Finite Element Method, multibody systems approaches and aerodynamic load calculations. The presented examples demonstrate the feasibility of such an implicit coupling approach.

Future developments will include improved bearing models which take into account the impact of coupled axial-radial-bending effects. These enhancements will be coupled with the presented approach in terms of further external computer programs. Concerning further improvements to the aero-elastic coupling, future developments will focus on the computation of aerodynamically induced velocities in the near and far field in terms of enhanced dynamic stall models and wake representations.

It is expected that the availability of more precise fatigue load spectra will contribute to improvements in the design of wind turbine power trains.

REFERENCES

AGMA Foundation the American Gear Manufacturers Association. *ANSI/AGMA/AWEA 6006-A03 - Standard for Design and Specification of Gearboxes for Wind Turbines*. AGMA Foundation the American Gear Manufacturers Association, Alexandria, VA, USA, 2003.

Amzallag C., Gerey J.P., Robert J.L., and Bahuaud J. Standardization of the rainflow counting method for fatigue analysis. *International Journal of Fatigue*, 16(4):287–293, 1994.

Anderson J.D. *Fundamentals of Aerodynamics*. McGraw-Hill, Inc., Boston, MA, USA, 1984.

Bathe K.J. *Finite Element Procedures in Engineering Analysis*. Prentice-Hall, Inc., Englewood Cliffs, NJ, USA, 1982.

Belytschko T. *An Overview of Semidiscretization and Time Integration Procedures*, pages 1–65. North-Holland, Amsterdam, the Netherlands, 1983.

Bishop N. and Sherratt F. Fatigue life prediction from power spectral density data. part 2 : Recent developments. *Environmental Engineering*, 2:11–19, 1989a.

Bishop N. and Sherratt F. A theoretical solution for the estimation of rainflow ranges from power spectral density data. *Fatigue & fracture engineering materials & Structures*, 13:311–326, 1990.

Bishop N.W. and Sherratt F. Fatigue life prediction from power spectral density data. part 1 : Traditional approaches. *Environmental Engineering*, 2:11–19, 1989b.

Bossanyi E.A. *GH-Bladed User Manual*. Garrad Hassan and Partners Limited, Bristol, UK, 2004. Issue 14.

Burton T., Sharpe D., Jenkins N., and Bossanyi E. *Wind Energy Handbook*. John Wiley and Sons Ltd., Chichester, UK, 2001.

Cardona A. Three dimensional gears modeling in multibody systems analysis. *International Journal for Numerical Methods in Engineering*, 40:357–381, 1997.

Cardona A. and Géradin M. Time integration of the equations of motion in mechanism analysis. *Computers and Structures*, 33(3):801–820, 1989.

Cardona A. and Géradin M. Modelling of super elements in mechanism analysis. *International Journal for Numerical Methods in Engineering*, 32:1565–1594, 1991.

Cardona A. and Géradin M. Numerical integration of second-order differential-algebraic systems in flexible mechanism dynamics. In *Computer-Aided Analysis of Rigid and Flexible Mechanical Systems*, volume E-268 of *Nato ASI Series*. 1994.

Cardona A., Géradin M., and Doan D.B. Rigid and flexible joint modelling in multibody dynamics using finite elements. *Computer Methods in Applied Mechanics and Engineering*, 89:395–418, 1991.

Cardona A. and Granville D. Flexible gear dynamics modelling in multibody analysis. In *5th US National Congress on Computational Mechanics Proceedings*, page 60. Boulder, CO, USA, 1999.

Cassano A. and Cardona A. A comparison between three variable step algorithms for the integration of the equations of motion in structural dynamics. *Latin American Research*, 21:187–197, 1991.

Craig R. and Bampton M. Coupling of substructures for dynamic analysis. *AIAA Journal*, 6(7):1313–1319, 1968.

Géradin M. and Cardona A. *Flexible Multibody Dynamics: A Finite Element Approach*. John Wiley and Sons Ltd, Chichester, UK, 2001.

Géradin M. and Rixen D. *Mechanical Vibrations, Theory and Application to Structural Dynamics*. John Wiley and Sons Ltd., Chichester, UK, 1993.

Germanischer Lloyd Windenergie GmbH. GL wind energy GmbH. section 7.1.3. GL wind technical note 068. requirements and recommendations for implementation and documentation of resonance analysis. In *Guideline for the Certification of Wind Turbines (Edition 2003 with Supplement 2004)*. Germanischer Lloyd Windenergie GmbH, Hamburg, Germany, 2006.

Gladwell I. and Thomas R.M. Variable-order variable-steps algorithms for second-order systems. part 2: The codes. *International Journal for Numerical Methods in Engineering*, 26:55–80, 1988.

Goudreau G.L. and Taylor R. Evaluation of numerical integration methods in elastodynamics. *Computer Methods in Applied Mechanics and Engineering*, 2(1):69–97, 1973.

Haug E.J. *Computer Aided Kinematics and Dynamics of Mechanical Systems, Volume I: Basic Methods*. Allyn and Bacon Series in Engineering. Simon & Schuster, Boston, MA, USA, 1989.

Heege A. Computation of wind turbine gearbox loads by coupled structural and mechanism analysis. In *NAFEMS World Congress 2005 Proceedings*. Malta, 2005.

Heege A. and Alart P. A frictional contact element for strongly curved contact problems. *International Journal for Numerical Methods in Engineering*, 39:165–184, 1996.

Heege A., Radovcic Y., and Betran J. Fatigue load computation of wind turbine gearboxes by coupled structural, mechanism and aerodynamic analysis. *DEWI Magazin*, 28:60–68, 2006a.

Heege A., Viladomiu P., Betran J., Radovcic Y., Latorre M., Cantons J.M., and Castell D. Impact of wind turbine drive train concepts on dynamic gearbox loads. In *DEWEK 2006 Proceedings*. 2006b.

Hilber H., Hughes T., and R.L.Taylor. Improved numerical dissipation for time integration algorithms in structural dynamics. *Earthquake Engineering & Structural Dynamics*, 5:283–292, 1977.

Hughes T. *The Finite Element Method: Linear Static and Dynamic Finite Element Analysis*. Prentice Hall, Englewood Cliffs, NJ, USA, 1987.

International Electrotechnical Commission. Wind turbine generator systems - part 1: Safety requirements. Technical Report IEC 61400-1, International Electrotechnical Commission, Geneva, Switzerland, 1997. Second edition.

J. K. and A P. *Low-Speed Aerodynamics: From Wing Theory to Panel Methods*. McGraw-Hill Book Co., New York, NY, USA, 1991.

Johnsen B. Praxisergebnisse aus schleswig-holstein: Getriebe- und generatorstörung betreffen

die megawattanlagen. In *Erneuerbare Energien*, page 36. Verlag/Hannover, Germany, 2004.

Leishman J.G. and Beddoes T.S. A semi- empirical model for dynamic stall. *Journal of the American Helicopter Society*, 128:461–471, 1989.

Lens E. *Energy Preserving/Decaying Time Integration Schemes for Multibody Systems Dynamics*. Ph.D. thesis, Universidad Nacional del Litoral, Argentina, 2006.

Lens E. and Cardona A. An energy Preserving/Decaying scheme for constrained nonlinear multibody systems. *Multibody System Dynamics*, 2007. *Status: online first. Published online: 28 February 2007*.

Manwell J.F., McGowan J.G., and Rogers A.L. *Wind Energy Explained*. John Wiley and Sons Ltd., Chichester, UK, 2002.

Øye S. Dynamic stall- simulated as time lag of separation. In *IEA Symposium on the Aerodynamics of Wind Turbines*. Harkwell, UK, 1990.

Øye S. FLEX 4 - simulation of wind turbine dynamics. In *Proceedings of the 28th IEA Meeting of Experts "State of the Art of Aerolelastic Codes for Wind Turbine Calculations"*, pages 71–76. Technical University of Denmark, Lyngby, Denmark, 1996.

Øye S., Schepers J., Heijdra J., Foussekis D., Smith R., Belessis M., Thomsen K., Larsen T., Kraan I., Visser B., Carlen I., Ganander H., and Drost L. Verification of european wind turbine design codes. VEWTDC: Final report. Technical Report ECN-C-01-055, Energy Research Centre of the Netherlands (ECN), 2003.

Peeters J. *Simulation of Dynamic Drive Train Loads in a Wind Turbine*. Ph.D. thesis, Katholieke Universiteit Leuven, Belgium, 2006.

Pitoiset X. *Méthodes Spectrales Pour Une Analyse En Fatigue Des Structures Métalliques Sous Chargements Aléatoires Multiaxiaux*. Ph.D. thesis, Université Libre de Bruxelles, 2001.

Samtech SA. *Samcef / Mecano V 12 User Manual*. Samtech SA, 2007.

Spera D.A., editor. *Wind Turbine Technology: Fundamental Concepts of Wind Turbine Engineering*. ASME press, New York, NY, USA, 1994.

Sutherland H.J. Fatigue case study and loading spectra for wind turbines. In *IEA Fatigue Experts Meeting*, pages 77–87. Sandia National Laboratories, Albuquerque, NM, USA, 1994.

Thomas R.M. and Gladwell I. Variable-order variable-steps algorithms for second-order systems. part 1: The methods. *International Journal for Numerical Methods in Engineering*, 26:39–53, 1988.

Veers S.P. Three-dimensional wind simulation. Technical Report SAND88-0152.UC-261, Sandia, 1988.

Wilson R.E. and Lissaman P.B.S. Applied aerodynamics of wind-power machines. Technical Report PB-238-595, Oregon State University, USA, 1974.